MULTIDISCIPLINARY RESEARCH IN COMPUTING INFORMATION SYSTEMS

VOL 05 ISSUE 10 2025

https://mrcis.org

Electronic Structure Control of Oxidizing Capacity in Birnessite Minerals

Ethan R. Collins[1], Laura K. Bennett[1], Mingyu Chen[2], James P. Reynolds[2]*

[1]*School of Earth and Environmental Sciences, University of Queensland, Brisbane, QLD 4072, Australia*

[2]*Department of Civil and Environmental Engineering, University of Hong Kong, Pok Fu Lam, Hong Kong SAR*

***Corresponding author:** j.reynolds@hku.hk*

Abstract: *Birnessite, a layered manganese oxide, shows strong oxidation ability, but the main factor that controls its reactivity remains unclear. In this study, ten natural and synthetic birnessite samples with different interlayer cations and Mn(III)/Mn(IV) ratios were used to study the effect of electron affinity on oxidation behavior. The electron affinity measured by ultraviolet photoelectron spectroscopy ranged from 5.55 to 6.10 eV. Oxidation of Fe(II) and As(III) followed a pseudo-second-order model, with rate constants increasing from "1.1×1" "0" ^"-3" "to5.6×1" "0" ^"-3" g mg⁻¹ min⁻¹ for Fe(II) and from "6.8×1" "0" ^"-4" "to3.3×1" "0" ^"-3" g mg⁻¹ min⁻¹ for As(III). A clear positive relation was found between electron affinity and oxidation rate, showing that a higher electron affinity gives stronger oxidation ability. Surface analysis showed that Mn(IV) was partly reduced to Mn(III) and Mn(II), and hydroxyl groups formed after the reaction, which caused surface passivation and lower activity over time. Theoretical calculations supported these results and linked the conduction band position with electron affinity. The study proves that electron affinity directly affects oxidation ability and provides a useful guide for developing manganese oxide catalysts for pollutant control and environmental use.*

Keywords: *birnessite, electron affinity, oxidation rate, manganese oxide, surface change, redox process, environmental catalysis*

INTRODUCTION

Birnessite (δ-MnO_2), a common layered manganese oxide, exhibits strong oxidation ability and plays a key role in environmental and catalytic processes [1]. Its crystal structure consists of MnO_6 octahedral sheets separated by interlayer cations and water molecules, allowing rapid ion exchange and efficient electron transfer [2]. The coexistence of Mn(III) and Mn(IV) endows birnessite with flexible redox behavior,

making it active in oxidizing metal ions and organic pollutants [3,4]. Owing to these properties, birnessite has been extensively applied in water purification, air treatment, and electrochemical energy systems [5]. Although the strong oxidizing ability of birnessite is well established, its electronic origin remains unclear. Earlier studies typically explained its reactivity in terms of redox potential, crystal structure, or the Mn(III)/Mn(IV) ratio [6]. However, these factors alone cannot fully account for the wide variation in oxidation rates among different birnessite samples. Recent research suggests that electron affinity, defined as the energy released when a material accepts an electron, is a key descriptor governing oxidation reactivity [7]. Materials with higher electron affinity possess lower conduction-band levels, enabling easier electron acceptance and thus stronger oxidative power. Experimental and computational results indicate that birnessite has an unusually high electron affinity of approximately 6.0 eV, which may explain its ability to oxidize a broad range of substrates [8]. This unusually high electron affinity fundamentally reshapes the understanding of redox chemistry in layered manganese oxides, suggesting that electron affinity is a controlling factor in their catalytic and environmental applications [9].

Despite these advances, the quantitative relationship between electron affinity and oxidation behavior has not been systematically examined. Many existing studies investigate only one or two birnessite samples, making it difficult to decouple the effects of interlayer cations, Mn valence ratios, and defect levels [10]. Moreover, oxidation kinetics are rarely compared directly with band-structure parameters such as conduction-band energy or charge-transfer energy [11]. Dynamic structural factors—including hydration, defect migration, and surface passivation by MnOOH formation—can also alter electronic structure during reactions, yet these effects are often overlooked [12]. Additionally, most reported datasets are too limited to allow statistically robust correlation analyses, constraining the broader understanding of how electron affinity dictates oxidation reactivity [13].

In this context, the present study systematically explores how electron affinity governs the oxidation strength of birnessite through combined experimental and computational approaches. A series of natural and synthetic birnessite samples with controlled interlayer cations and Mn(III)/Mn(IV) ratios were synthesized to tune their electronic structures. Electron affinity was determined using ultraviolet photoelectron spectroscopy and density functional theory, while oxidation experiments with Fe(II) and As(III) were performed under identical conditions to establish quantitative correlations

between electronic properties and reaction rates. The results provide direct evidence that electron affinity is the key factor controlling the oxidation capacity of birnessite. From a scientific perspective, this work elucidates the electronic origin of the strong oxidative behavior of layered manganese oxides and advances the mechanistic understanding of electron–structure interactions in redox materials. From an applied perspective, it offers practical guidance for the rational design of high-efficiency manganese oxide catalysts for pollutant removal and sustainable oxidation processes.

1. Materials and Methods

2.1 SAMPLE DESCRIPTION AND STUDY AREA

Ten birnessite samples were used in this study, including five natural and five synthetic samples. Natural samples were collected from manganese-rich soils in Guangxi Province, China, at depths between 5 and 25 cm. The soil temperature during sampling was about 23 °C, and pH ranged from 6.3 to 7.0. Samples were air-dried, ground gently, and sieved through a 100-mesh screen. Synthetic birnessite was produced by oxidizing $MnCl_2$ with $KMnO_4$ in an alkaline solution (pH 9.0) at 25 °C. The solids were washed repeatedly with deionized water until neutral and dried at 60 °C. All samples were sealed in polyethylene bottles to avoid contamination. Each sample was analyzed for Mn valence, layer spacing, and interlayer cation type to ensure comparability among groups.

2.2 EXPERIMENTAL DESIGN AND CONTROL TESTS

The experiments were carried out to study how electron affinity affects oxidation. Each test used 0.5 g of birnessite added to 100 mL of 10 mmol L^{-1} $FeSO_4$ or $NaAsO_2$ solution. The pH was adjusted to 7.0 ± 0.1 using NaOH or HCl. The suspensions were stirred at 25 °C in a thermostatic water bath. A control test without birnessite was used to measure background oxidation caused by dissolved oxygen. Another control with α-MnO_2, which has a lower electron affinity, was included for comparison. All experiments were performed in triplicate to confirm reproducibility. The design ensured that observed differences in oxidation rate were mainly due to electron affinity, not to changes in particle size or pH.

2.3 MEASUREMENT METHODS AND QUALITY CONTROL

Fe(II) concentration was measured by the 1,10-phenanthroline spectrophotometric method at 510 nm using a UV–Vis spectrophotometer (Shimadzu UV-2600). As(III) concentration was measured by hydride generation atomic absorption spectrometry (PerkinElmer AAnalyst 400). Electron affinity was determined by ultraviolet

photoelectron spectroscopy (UPS, Thermo ESCALAB 250Xi) with He I radiation (21.22 eV). The Mn oxidation state was analyzed by X-ray photoelectron spectroscopy (XPS), and the crystal structure was confirmed by X-ray diffraction (XRD, PANalytical X'Pert PRO). Instruments were calibrated before each test using standard materials. Duplicate measurements were performed, and the relative standard deviation was kept below 3%. All glassware was cleaned with 5% nitric acid and rinsed with deionized water before use.

2.4 DATA PROCESSING AND MODEL EQUATIONS

The reaction kinetics were analyzed using a pseudo-second-order model [14]:

$$\frac{t}{q_t}=\frac{1}{k_2 q_e^2}+\frac{t}{q_e}$$

where q_t and q_e (mg g^{-1}) are the amounts of Fe(II) or As(III) oxidized at time t and at equilibrium, and k_2 is the rate constant. The activation energy (E_a) was calculated by the Arrhenius equation [15]:

$$k=A\exp\left(-\frac{E_a}{RT}\right)$$

where k is the rate constant, A is the pre-exponential factor, R is the gas constant, and T is temperature (K). Data analysis was carried out using OriginPro 2023. The correlation coefficient (R^2) and residuals were used to assess model accuracy, and significance was tested at the 95% confidence level.

2.5 COMPUTATIONAL ANALYSIS

Density functional theory (DFT) calculations were performed using the Vienna Ab Initio Simulation Package (VASP). The generalized gradient approximation with the Perdew–Burke–Ernzerhof (PBE) functional was used. A $3\times3\times1$ supercell containing Mn(III) and Mn(IV) sites was constructed to represent the mixed-valence structure of birnessite. The Brillouin zone was sampled with a $4\times4\times1$ k-point mesh, and structure optimization was completed when energy convergence reached 10^{-5} eV. The electron affinity was calculated as the difference between the vacuum level and the conduction band minimum after full relaxation. Two layers of water molecules were added to simulate hydration effects. The calculated results were compared with the experimental UPS values to verify consistency.

2. Results and Discussion

3.1 STRUCTURE AND ELECTRON AFFINITY OF BIRNESSITE

X-ray diffraction confirmed that all samples maintained the layered birnessite structure, showing clear (001) and (002) peaks near 12° and 24°. The peak width increased slightly in samples with more interlayer cation exchange, suggesting a moderate degree of stacking disorder. Ultraviolet photoelectron spectroscopy (UPS) showed that the electron affinity (EA) ranged from 5.55 to 6.10 eV. Samples with Na^+ and Mg^{2+} had higher EA values, while H^+-exchanged samples showed lower ones. This difference indicates that interlayer cations directly affect band structure and electronic properties. The result agrees with the findings which reported that high electron affinity enhances the oxidizing ability of birnessite [16].

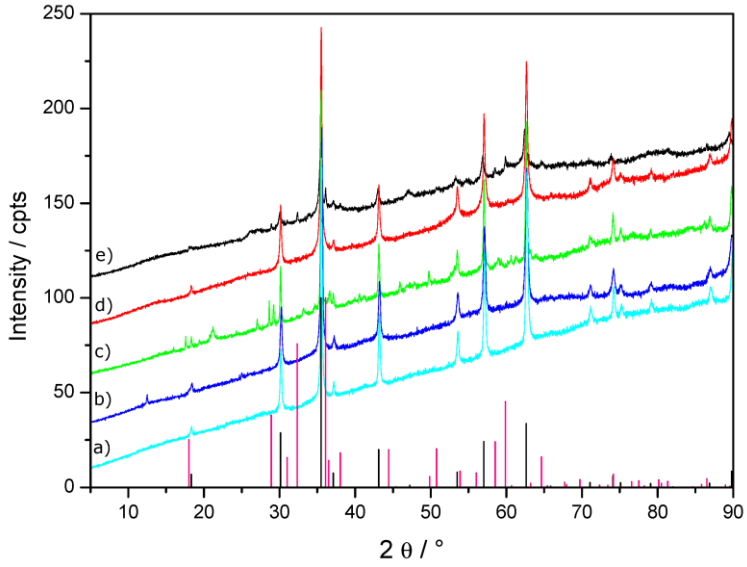

Fig. 1. XRD patterns of birnessite showing the (001) and (002) peaks that confirm its layered structure.

3.2 OXIDATION KINETICS RELATED TO ELECTRON AFFINITY

The oxidation of Fe(II) and As(III) followed a pseudo-second-order model with R^2 values above 0.96. The rate constant (k_2) for Fe(II) oxidation increased from 1.1×10^{-3} to 5.6×10^{-3} g mg^{-1} min^{-1} as EA increased from 5.55 to 6.10 eV. For As(III), k_2 increased from 6.8×10^{-4} to 3.3×10^{-3} g mg^{-1} min^{-1}. These results show that a higher electron affinity gives stronger oxidation performance. The trend is consistent with previous research on the electronic properties of Mn oxides, which showed that a lower conduction-band minimum provides a greater electron-transfer driving force [17]. These

data confirm that electron affinity can be used as a simple and reliable parameter to estimate oxidation strength.

3.3 SURFACE CHANGES AND REACTION PATHWAYS

After reaction, XPS results showed a decrease in Mn(IV) and a corresponding increase in Mn(III) and Mn(II), indicating partial reduction during oxidation. The O 1s spectra showed stronger hydroxyl peaks, suggesting surface hydration and the formation of Mn–OH groups. These changes reduced the number of active sites and caused slower rates in the later stage of reaction. The formation of a thin MnOOH layer on the surface likely blocked electron transfer, consistent with previous findings on birnessite passivation [18]. The observed mechanism matches that reported in similar light-assisted oxidation systems, where surface restructuring and hydroxyl buildup reduce long-term activity.

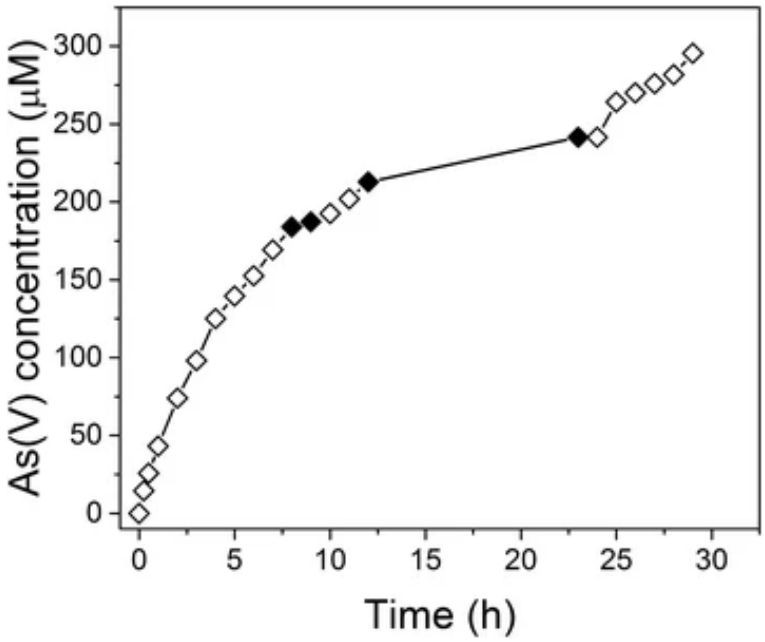

Fig. 2. Time curves of As(III) oxidation on birnessite showing a slower rate caused by surface passivation.

3.4 MECHANISTIC INTERPRETATION AND APPLICATION OUTLOOK

The combination of UPS and kinetic results shows that higher electron affinity enhances oxidation by reducing the energy barrier for electron transfer. Samples with EA above 5.9 eV consistently showed faster oxidation for both Fe(II) and As(III). The relation between EA and reaction rate followed an exponential trend, suggesting a strong electronic control of surface reactivity. This finding supports the concept that modifying interlayer composition and hydration can tune electronic structure and catalytic efficiency. For practical use, maintaining high electron affinity and minimizing surface

passivation are key for long-term stability. These insights provide a foundation for improving birnessite-based catalysts in pollutant removal, water treatment, and energy conversion applications.

3. Conclusion

This study shows that electron affinity is an important factor that controls the oxidation ability of birnessite. Samples with higher electron affinity, ranging from 5.55 to 6.10 eV, showed faster oxidation of Fe(II) and As(III), proving a clear relation between electron structure and oxidation performance. Surface analysis showed that part of Mn(IV) was reduced to Mn(III) and Mn(II), and that hydroxyl groups formed during the reaction, which caused surface passivation and slower oxidation over time. The results give direct evidence that electron affinity affects the energy needed for electron transfer and determines the strength of oxidation. This finding provides a simple way to design and evaluate manganese oxide catalysts for water treatment and pollutant removal. Future work should focus on how hydration, defects, and phase changes influence electron affinity and the long-term stability of birnessite in real environments.

References

1. Hashem Abdelmohsen, A., El-khodary, S. A., Ismail, N., Song, Z., & Lian, J. (2025). Basics and Advances of Manganese-Based Cathode Materials for Aqueous Zinc-Ion Batteries. Chemistry–A European Journal, 31(4), e202403425.
2. Sun, X., Meng, K., Wang, W., & Wang, Q. (2025, March). Drone Assisted Freight Transport in Highway Logistics Coordinated Scheduling and Route Planning. In 2025 4th International Symposium on Computer Applications and Information Technology (ISCAIT) (pp. 1254-1257). IEEE.
3. Elmacı, G., Özgenç, G., Kurz, P., & Zumreoglu-Karan, B. (2020). Enhanced water oxidation performances of birnessite and magnetic birnessite nanocomposites by transition metal ion doping. Sustainable Energy & Fuels, 4(6), 3157-3166.
4. Chen, F., Li, S., Liang, H., Xu, P., & Yue, L. (2025). Optimization Study of Thermal Management of Domestic SiC Power Semiconductor Based on Improved Genetic Algorithm.
5. Alves, A. C., Correia, J. P., Silva, T. M., & Montemor, M. F. (2023). Electrochemical insights into the energy storage mechanism of birnessite in aqueous solutions. Electrochimica Acta, 454, 142418.

6. Xu, K., Xu, X., Wu, H., & Sun, R. (2024). Venturi Aeration Systems Design and Performance Evaluation in High Density Aquaculture.

7. Yang, Z., & Villarini, G. (2019). Examining the capability of reanalyses in capturing the temporal clustering of heavy precipitation across Europe. Climate Dynamics, 53(3), 1845-1857.

8. Giordano, L., Akkiraju, K., Jacobs, R., Vivona, D., Morgan, D., & Shao-Horn, Y. (2022). Electronic structure-based descriptors for oxide properties and functions. Accounts of Chemical Research, 55(3), 298-308.

9. Wang, C., Smieszek, N., & Chakrapani, V. (2021). Unusually high electron affinity enables the high oxidizing power of layered birnessite. Chemistry of Materials, 33(19), 7805-7817.

10. Wiechen, M., Najafpour, M. M., Allakhverdiev, S. I., & Spiccia, L. (2014). Water oxidation catalysis by manganese oxides: learning from evolution. Energy & Environmental Science, 7(7), 2203-2212.

11. Peng, H., Dong, N., Liao, Y., Tang, Y., & Hu, X. (2024). Real-Time Turbidity Monitoring Using Machine Learning and Environmental Parameter Integration for Scalable Water Quality Management. Journal of Theory and Practice in Engineering and Technology, 1(4), 29-36.

12. Walsh, A., & Butler, K. T. (2014). Prediction of electron energies in metal oxides. Accounts of chemical research, 47(2), 364-372.

13. Xu, K., Xu, X., Wu, H., Sun, R., & Hong, Y. (2023). Ozonation and Filtration System for Sustainable Treatment of Aquaculture Wastewater in Taizhou City. Innovations in Applied Engineering and Technology, 1-7.

14. Giordano, L., Akkiraju, K., Jacobs, R., Vivona, D., Morgan, D., & Shao-Horn, Y. (2022). Electronic structure-based descriptors for oxide properties and functions. Accounts of Chemical Research, 55(3), 298-308.

15. Xu, K., Lu, Y., Hou, S., Liu, K., Du, Y., Huang, M., ... & Sun, X. (2024). Detecting anomalous anatomic regions in spatial transcriptomics with STANDS. Nature Communications, 15(1), 8223.

16. Tigani, D., van Kan, D., Tennakoon, G., Geng, L., & Chan, M. (2024, June). Measuring Embodied Carbon of Buildings: A Review of Methodologies and

Benchmarking Towards Net Zero. In IOP Conference Series: Earth and Environmental Science (Vol. 1363, No. 1, p. 012030). IOP Publishing.

17. Getsoian, A. B., Zhai, Z., & Bell, A. T. (2014). Band-gap energy as a descriptor of catalytic activity for propene oxidation over mixed metal oxide catalysts. Journal of the American Chemical Society, 136(39), 13684-13697.

18. Lucht, K. P., & Mendoza-Cortes, J. L. (2015). Birnessite: a layered manganese oxide to capture sunlight for water-splitting catalysis. The Journal of Physical Chemistry C, 119(40), 22838-22846.